

Effective level attraction and magnetic flux-induced negative differential conductance in two double quantum dot molecules embedded in an Aharonov-Bohm ring

M. L. Ladrón de Guevara¹, Gustavo A. Lara², and P. A. Orellana¹

¹*Departamento de Física, Universidad Católica del Norte, Casilla 1280, Antofagasta, Chile and*

²*Departamento de Física, Universidad de Antofagasta, Casilla 170, Antofagasta, Chile*

(Dated: September 3, 2021)

We study transport of non-interacting electrons through two quantum dot molecules embedded in an Aharonov-Bohm interferometer. The system in equilibrium exhibits bound states in the continuum (BIC) and total suppression of transmission. It also shows a magnetic flux-dependent effective level attraction and lines of perfect transmission when the intramolecular coupling is weak. Out of equilibrium, the current displays two kind of negative differential conductance (NDC) regions, which have different origins. One is generated by the usual mechanism of the NDC arising in a double quantum dot system. The other is induced by the magnetic flux, and it occurs at small voltages and for a well definite range of the intramolecular couplings. We explain this effect in terms of the level attraction displayed by the system.

PACS numbers: 73.21.La; 73.63.Kv; 85.35.Ds; 85.35.Be

I. INTRODUCTION

Advances in experimental techniques at the nanometer scale have allowed to realize and manipulate quantum dots in a controlled way¹. This has permitted to study in these systems a wide spectrum of phenomena², as well as to take advantage of some properties of quantum dots to build nano-devices, such as rectifiers, amplifiers, lasers, and others^{3,4,5,6}. For their similitude with atoms, quantum dots are often viewed as artificial atoms, and two or more coupled quantum dots as artificial molecules. Multiple quantum dot systems, and in particular the double quantum dot (DQD) molecule⁷, are of particular importance, because they are more controllable than single quantum dots. Moreover, they admit different kind of connections to leads. Initially, most of studies considered serial DQDs⁸, but posteriorly parallel^{9,10,11} and T-shaped^{12,13} configurations were also examined, emerging quantum interference effects due to the existence of different electronic paths. Much attention has received the DQD molecule embedded in an Aharonov-Bohm ring, where the presence of a magnetic flux adds a new tool in the control of the transport properties. Aharonov-Bohm (AB) oscillations and Fano effect in a DQD molecule embedded in a ring have been observed experimentally^{9,14,15}. There is much theoretical work supporting these experiments and exploring new phenomena in the DQD embedded in a ring. Fano resonances and the magnetic-flux controllability of transport are examined, for example, in Refs. 10,11,16,17,18,19, both in presence and the absence of electronic correlations. The existence of bound states in the continuum (BICs) is discussed in Refs. 10,16. The interplay between quantum interference and Kondo physics in the parallel-coupled DQD has been also explored^{20,21}. A closely related system which has received attention is the AB interferometer with two embedded quantum dots^{22,23}. Kubala and König studied equilibrium transport in this system, finding an *effective flux-dependent level attraction* in the lin-

ear conductance²². This effect is caused by the renormalization of levels by the leads.

From the applicability point of view, an interesting feature exhibited by the transport through quantum dots is the negative differential conductance (NDC)²⁴. NDC has been studied in single as well as in double quantum dot systems, and it has applications in amplifiers and oscillators in the microwave, mm-wave and Terahertz frequency ranges²⁵. In multilevels quantum dots NDC can occur when states have different couplings to the leads^{26,27,28,29}. In a serial DQD, NDC can be produced when the bias breaks the transmission channel extended along the system³⁰. Other theoretical works on generation of NDC in DQD connected in series are Refs. 31,32,33,34,35. In a DQD embedded in an Aharonov-ring, magnetic-flux-induced NDC was found in the strong interdot repulsion regime¹⁹. A similar result was found by Mourokh and Smirnov in a DQD molecule with three terminals³⁶. Recently, it was reported NDC induced by the electronic correlation in a side-coupled DQD³⁷.

In this work we study equilibrium and non-equilibrium transport through two quantum dot molecules embedded in an Aharonov-Bohm interferometer. We obtain analytical expressions for the transmission and we calculate numerically the current at zero temperature. In equilibrium, the transmission exhibits Fano resonances, total reflection, and suppressed peaks as a manifestation of bound states in the continuum. Moreover, we find for small intramolecular couplings a flux-dependent effective level attraction and lines of perfect transmission. This effect occurs no matter how weakly coupled are the quantum dots forming each molecule.

In the non-equilibrium regime, we identify two kind of NDC regions in the I - V characteristics, occurring at different scales and of different origin. One is generated by the usual mechanism of the NDC in a double quantum dot systems, and it is independent of the magnetic flux. The current will increase or decrease with voltage, depending on whether the voltage makes the levels of the

different quantum dots become aligned or not aligned. The second NDC region is induced by the magnetic flux, and it occurs only for a definite range of intramolecular couplings. An abrupt rise of current occurs for small bias voltages as consequence of the effective level attraction of the hybridized levels produced by the magnetic flux. The decrease of current is result of the destruction of this effect when the bias voltage is increased.

II. MODEL

The system under consideration is shown in Fig. 1. Two equal double quantum dot molecules are embedded in an Aharonov-Bohm ring, which is attached to large contacts through one-dimensional leads. Equilibrium transport in a similar configuration with additional connections between dots was studied by Li *et al.*³⁸. The left and right contacts are in thermodynamic equilibrium with thermodynamical potentials μ_L and μ_R , respectively. The leads are assumed to be ballistic conductors. We assume that a bias voltage V/e is applied between source and drain such that the site energy is $V/2$ for the left lead and $-V/2$ for the right lead. We consider only one level relevant in each of the quantum dots. The system is modeled by a non-interacting Anderson Hamiltonian, which can be written as

$$H = H_M + H_0 + H_I, \quad (1)$$

where H_M describes the dynamics of the isolate molecules,

$$H_M = \sum_{\alpha=+,-} \sum_{i=A,B} \varepsilon_i d_{i\alpha}^\dagger d_{i\alpha} + \sum_{\alpha=+,-} (t_\alpha d_{A,\alpha}^\dagger d_{B,\alpha} + t_\alpha^* d_{B,\alpha}^\dagger d_{A,\alpha}), \quad (2)$$

where $\varepsilon_{A(B)}$ is the level energy of the left (right) quantum dot in the molecule α ($\alpha = +, -$); $d_{i,\alpha}$ ($d_{i,\alpha}^\dagger$) annihilates (creates) an electron in dot i in the molecule α , and t_α is the intramolecular tunneling hopping. H_0 is the Hamiltonian for the noninteracting electrons in the leads,

$$H_0 = \frac{V}{2} \sum_{i=-N}^{-1} c_i^\dagger c_i + v \sum_{i=-N}^{-1} (c_i^\dagger c_{i-1} + c_{i-1}^\dagger c_i) - \frac{V}{2} \sum_{i=1}^N c_i^\dagger c_i + v \sum_{i=1}^N (c_i^\dagger c_{i+1} + c_{i+1}^\dagger c_i)$$

where c_i (c_i^\dagger) is the annihilation (creation) operator of an electron in the site i -th of the leads, and v the hopping between sites in the leads. The term H_I accounts for the tunneling between molecules and leads,

$$H_I = - \sum_{\alpha=+,-} (V_\alpha^A d_{A\alpha}^\dagger c_{-1} + V_\alpha^{A*} c_{-1}^\dagger d_{A\alpha}) - \sum_{\alpha=+,-} (V_\alpha^B d_{B\alpha}^\dagger c_1 + V_\alpha^{B*} c_1^\dagger d_{B\alpha})$$

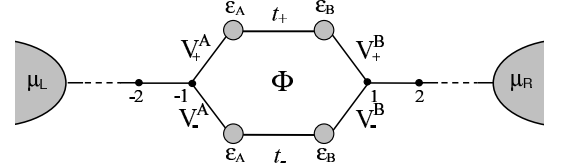


FIG. 1: Two double quantum dot molecules embedded in parallel in an Aharonov-Bohm interferometer

with $V_\alpha^{A(B)}$, the tunneling coupling connecting the left (right) dot of the α -th molecule with the left (right) lead. We restrict to the case in which there is not magnetic field acting directly on the electrons, so that the situation will be identical for the two values of spin. Therefore in what follows we omit the spin index.

In presence of a magnetic flux threading the ring, and using gauge invariance, we add the Aharonov-Bohm phase $\phi = 2\pi\Phi/\Phi_0$ around the ring by the replacement

$$V_+^A = t_A e^{-i\phi/6}, \quad t_+ = t_c e^{-i\phi/6}, \quad V_+^B = t_B e^{-i\phi/6}, \\ V_-^A = t_A e^{i\phi/6}, \quad t_- = t_c e^{i\phi/6}, \quad V_-^B = t_B e^{i\phi/6}, \quad (3)$$

with $\Phi_0 = h/e$ the flux quantum. We look for the steady states $|\psi_k\rangle$ of the whole Hamiltonian H . The Hamiltonian describing the leads, H_0 , corresponds to a free-particle Hamiltonian on a lattice, the eigenfunctions being Bloch functions

$$|k_\beta\rangle = \sum_j e^{ik_\beta j} |j\rangle, \quad \beta = L, R, \quad (4)$$

where $|k_\beta\rangle$ is the momentum eigenstate and $|j\rangle$ a Wannier state localized at the j -th site. The corresponding dispersion relations are $\varepsilon = V/2 - 2v \cos k_L$, for the electrons originated in the left contact, and $\varepsilon = -V/2 - 2v \cos k_R$ for those originated in the right contact. The eigenstates of the entire Hamiltonian can be written as

$$|\psi_k\rangle = \sum_{j=-N}^{-1} a_j^k |j\rangle + \sum_{\alpha=+,-} \sum_{i=A,B} b_{i,\alpha}^k |i,\alpha\rangle + \sum_{j=1}^N a_j^k |j\rangle \quad (5)$$

We assume electrons as described by a plane wave incident from the far left (right) with unit amplitude, reflection amplitude r (r'), and transmission amplitude t (t'). Thus, for electrons incident from the left,

$$a_j^{kL} = \begin{cases} e^{ik_L j} + r e^{-ik_L j} & j \leq -1 \\ t e^{ik_R j}, & j \geq 1 \end{cases} \quad (6)$$

and for electrons incident from the right,

$$a_j^{kR} = \begin{cases} e^{-ik_R j} + r' e^{ik_R j} & j \geq 1 \\ t' e^{-ik_L j}, & j \leq -1 \end{cases} \quad (7)$$

where the two contributions are independent. Inserting Eqs. (5),(6) and (7) in the Schrödinger equation $H|\psi_k\rangle =$

$E_k|\psi_k\rangle$, we can solve for a_j^k and $b_{i,\alpha}^k$. We are interested in the transmission and the current through the system for an applied voltage V/e between contacts. We center in the the symmetrical configuration, that is, equal left and right dot-lead couplings, $t_A = t_B$. Additionally, the energies of the quantum dots are $\varepsilon_A = \mu_L$ and $\varepsilon_B = \mu_R$.

The current in the leads is given by

$$I = \frac{2ieV}{\hbar} \left(\langle c_{j+1}^\dagger c_j \rangle - \langle c_j^\dagger c_{j+1} \rangle \right), \quad (8)$$

where

$$\langle c_i^\dagger c_j \rangle = \frac{1}{2} \sum_{\alpha=\{L,R\}} \frac{1}{N} \sum_{k_\alpha} f(\varepsilon_{k_\alpha} - \mu_\alpha) a_i^{k_\alpha*} a_j^{k_\alpha}. \quad (9)$$

We assume that the voltage drop occurs only between the dot A and the dot B , so that the energies of the quantum dots are equal to the site energies of the adjacent leads, $\varepsilon_A = V/2$ and $\varepsilon_B = -V/2$. At zero temperature, the states that contribute to the net current are the states of the left lead with energies between $\mu_R = -V/2$ and $\mu_L = V/2$. Evaluating (8)-(9), we arrive to the following expression for the current

$$I(V) = \frac{2e}{h} \int_{-V/2}^{V/2} T(\varepsilon) d\varepsilon, \quad (10)$$

where $T(\varepsilon)$ is the transmission. We have assumed that the Fermi level in equilibrium is equal to 0.

III. RESULTS

The transmission probability can be written in the simple form

$$T(\varepsilon) = \frac{4t_c^2\Gamma^2(\Delta\varepsilon)^4 \cos^2 \phi/2}{[(\Delta\varepsilon)^4 + \Gamma^2(\varepsilon - q)^2][(\Delta\varepsilon)^4 + \Gamma^2(\varepsilon + q)^2]} \quad (11)$$

where $(\Delta\varepsilon)^2 = \varepsilon^2 - p^2$, with $p^2 = (V/2)^2 + t_c^2$ and $q^2 = (V/2)^2 + t_c^2 \cos^2(\phi/2)$, where $\Gamma = 4\pi t_A^2 \rho(0)$ is the characteristic line width, with $\rho(0)$ the density of states in the leads at the Fermi level. It is evident from the expression (11) that the transmission has a period $\Delta\phi = 2\pi$ ($\Delta\Phi = \Phi_0$). On the other hand, it is totally suppressed, both in and out of equilibrium, when ϕ is an odd multiple of π ($\Phi = n\Phi_0/2$, n odd). This fully destructive interference effect for this value of ϕ is expected, since in the absence of magnetic flux the upper and lower paths are equivalent, then the magnetic flux introduces in the wave function a phase $-\pi/2$ along one arm and $\pi/2$ along the other. The total suppression of transmission was discussed in an Aharonov-Bohm interferometer with two quantum dots, in equilibrium²².

A. Equilibrium transport

The equilibrium transmission is obtained from Eqs. (11)-(13) by making $V = 0$. Let us first analyze the

action of the magnetic flux in the conductance $G = (2e^2/h)T(0)$. This is given by

$$G = \frac{2e^2}{h} \frac{4 \cos^2(\pi\Phi/\Phi_0)(t_c/\Gamma)^2}{[\cos^2(\pi\Phi/\Phi_0) + (t_c/\Gamma)^2]^2}. \quad (12)$$

We distinguish in Eq. (12) two different behaviors. When $t_c \leq \Gamma$ there is always a value of Φ for which $G = 2e^2/h$, while when $t_c > \Gamma$ this never occurs. These behaviors are illustrated in Fig. 2, which shows the conductance versus the magnetic flux for two different values of the t_c . For $t_c = 0.25\Gamma$, the conductance reaches the max-

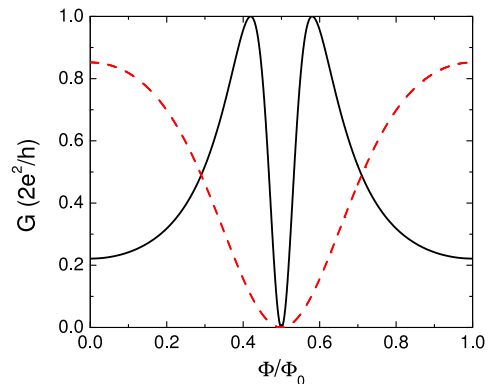


FIG. 2: (Color online) Conductance versus magnetic flux for $t_c = 0.25\Gamma$ (solid line) and $t_c = 1.5\Gamma$ (dash line).

imum $G = 2e^2/h$ in the interval $\Phi = 0$ to $\Phi = \Phi_0/2$, being symmetric around $\Phi_0/2$. Such a maximum occurs at $\varepsilon = \arccos(t_c/\Gamma)\Phi_0/\pi$. Similar features are found for any value of $t_c \leq \Gamma$, no matter how small it is. This is a remarkable result, taking into account that for a molecule in series the conductance, proportional to t_c^2 , gets progressively smaller as t_c decreases⁷. In contrast, for $t_c > \Gamma$ the conductance decays monotonously with Φ in the same interval, never reaching the quantum limit.

The occurrence of maximum conductance for small values of t_c is associated to an effective level attraction of the hybridized levels, similar to the discussed in Ref. 22 in an Aharonov-Bohm interferometer with two single-level quantum dots. This effect is illustrated in Fig. 3, which shows transmission versus energy for $t_c = 0.25\Gamma$. In the absence of magnetic flux, the transmission behaves qualitatively as that of the DQD in series. In Fig. 3a (dash line), t_c is small and a single and flat peak is observed. The hybridized states are not resolved yet, which is the usual for a molecule in series with small t_c . However, two BICs are occurring, similarly to what happen for a DQD embedded in an AB ring^{10,16}. In other words, two of the hybridized states are localized and do not participate of transmission. This situation repeats whenever $\Phi = n\Phi_0$ (n integer). When the flux is on, the BICs are replaced by two Fano resonances, as seen in the rest of Figs. 3. The Fano peaks reach $T = 1$.

In the sequence from Fig. 3a to Fig. 3d it can be observed the flux-controlled level attraction between hybridized states. As Φ is increased from 0 to $\Phi_0/2$ the

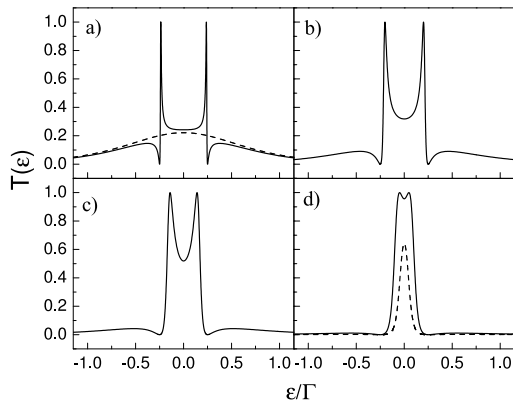


FIG. 3: Transmission versus energy for $t_c = 0.25\Gamma$ and a) $\Phi = 0$ (dash line) and $\Phi = 0.1\Phi_0$ (solid line), b) $\Phi = 0.2\Phi_0$, c) $\Phi = 0.3\Phi_0$, d) $\Phi = 0.4\Phi_0$ (solid line) and $\Phi = 0.46\Phi_0$ (dash line).

Fano peaks get progressively closer to each other until overlapping completely, the transmission decaying when Φ is close to $\Phi_0/2$ (dash line in Fig. 3d), until vanishing. The value $2e^2/h$ in the conductance shown above is reached when the two peaks overlap totally. In contrast, for $t_c = 1.5\Gamma$ the level attraction is not significant, as observed in Fig. 4.

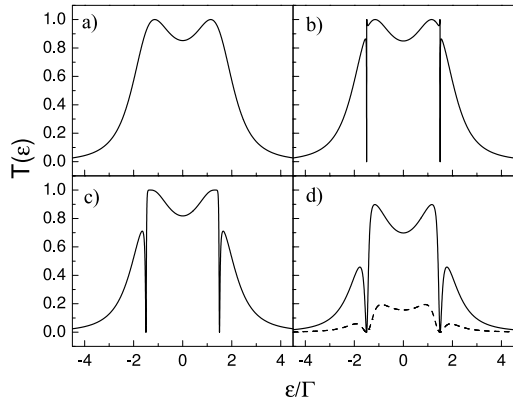


FIG. 4: Transmission versus energy for $t_c = 1.5\Gamma$ and a) $\Phi = 0$, b) $\Phi = 0.03\Phi_0$, c) $\Phi = 0.1\Phi_0$, d) $\Phi = 0.2\Phi_0$ (solid line) and $\Phi = 0.4\Phi_0$ (dash line).

It follows from Eq. 11 that perfect transmission takes place at energies obeying the following equation

$$\varepsilon^4 - \varepsilon^2(2t_c^2 - \Gamma^2) + t_c^2[t_c^2 - \Gamma^2 \cos^2(\phi/2)] = 0, \quad (13)$$

with two pair of solutions

$$\varepsilon_{\pm}^{\pm} = \pm[A + B^{1/2}]^{1/2}, \quad \varepsilon_{\pm}^{\mp} = \pm[A - B^{1/2}]^{1/2} \quad (14)$$

with $A = t_c^2 - \Gamma^2/2$ and $B = \Gamma^2 - 4t_c^2 \sin^2(\phi/2)$. Fig. 5 shows the positions of the $T = 1$ peaks for different values of $t_c \leq \Gamma/\sqrt{2}$. These correspond to ε_1^+ and ε_1^- , the only real solutions of Eq. (13). In the three cases the peaks positions shift progressively to the center of

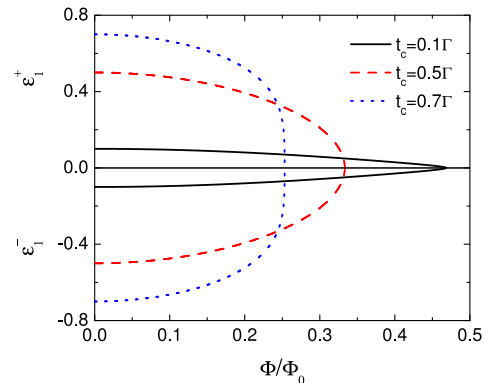


FIG. 5: (Color online) Positions of the $T = 1$ peaks for different values of $t_c \leq \Gamma/\sqrt{2}$.

the band as Φ increases. The peaks meet at $\varepsilon = 0$ at $\Phi = \arccos(t_c/\Gamma)\Phi_0/\pi$. The situation slightly changes when $\Gamma/\sqrt{2} < t_c \leq \Gamma$, where two new real solutions of Eq. (13) arise in the interval $\arccos(t_c/\Gamma)\Phi_0/\pi < \Phi \leq \arccos(1 - \Gamma^2/2t_c^2)\Phi_0/2\pi$, while ε_1^+ and ε_1^- become real for all $\Phi \leq \arccos(1 - \Gamma^2/2t_c^2)\Phi_0/2\pi$. This is illustrated in Fig. 6 for $t_c = 0.8\Gamma$ and $t_c = \Gamma$. The solutions ε_1^+ and ε_1^- never meet, but ε_2^+ and ε_2^- do so at $\varepsilon = 0$, being responsible of the conductance $G = 2e^2/h$ for these values of t_c . When $t_c > \Gamma$ there are four $T = 1$ peaks when $\Phi \leq \arccos(1 - \Gamma^2/2t_c^2)\Phi_0/2\pi$. These peaks never reach the center of the band, as shown for $t_c = 1.5\Gamma$.

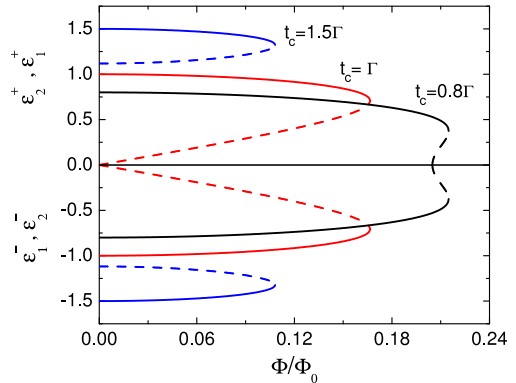


FIG. 6: Positions of the maxima of transmission for different values of $t_c > \Gamma/\sqrt{2}$. The solid lines correspond to ε_1^+ and ε_1^- , and the dash lines to ε_2^+ and ε_2^- .

We show below that the flux-dependent level attraction and the complete overlapping of resonances present for small values of t_c strongly influence the behavior of the non-equilibrium transport.

B. Non-equilibrium transport

Let us now consider a voltage V applied between contacts and let us study the current in the leads. Fig. 7 (upper panel) shows the current-voltage characteristics

for $\Phi = 0$ and different values of intramolecular couplings.

In all cases the current-voltage characteristics displays a peak, with the corresponding region of NDC. This feature occurs analogously to the observed in the serial DQD³⁰. The current increases when the bias allows a transmission channel exists along the left and right sides of the system. If the bias continues to increase, the channel is destroyed resulting in the drop of current. On the other hand, as occurs for quantum dots connected in series, in general larger values of t_c give larger values of the current for the same voltage.

The existence of a magnetic flux produces changes in the I - V characteristics which become important when $t_c < \Gamma/\sqrt{2}$ and Φ is within an interval close to $\Phi_0/2$, as illustrated in Fig. 7 (lower panel), where $\Phi = 0.46\Phi_0$. We observe sharper current peaks at lower voltages as compared to the case $\Phi = 0$. The abrupt increase of the

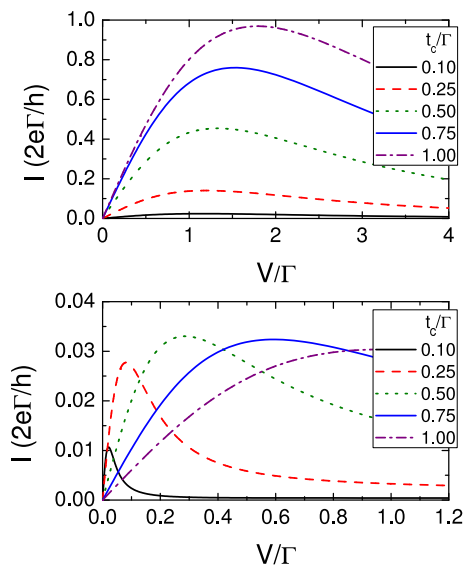


FIG. 7: (Color online) I - V characteristics for $\Phi = 0$ (upper panel) and $\Phi = 0.46\Phi_0$ (lower panel), and $t_c = 0.1\Gamma$ (solid line), $t_c = 0.25\Gamma$ (dash line), $t_c = 0.5\Gamma$ (dotted line), $t_c = 0.75\Gamma$ (dash-dotted line), $t_c = \Gamma$ (short dash line).

current at low voltages for small t_c is consequence of the level attraction discussed for zero bias. To visualize this we have plotted in Fig. 8 the I - V characteristics for a fixed t_c and Φ (left panel), and the transmission spectra associated to the bias voltages indicated in the current curve (right panel). As observed, for small bias (cases 1-3) the transmission keeps large in all the transport region ($-V/2 < \varepsilon < V/2$), due to the existence of two overlapped resonances close to each other. Larger bias voltages make the heights of the resonances fall, so that the transmission in all the window of transport becomes smaller, occurring the observed decrease in the current. A further insight of this is obtained through the density of states of the left and right quantum dots. Fig. 9 shows the left and right quantum dots DOS for the same param-

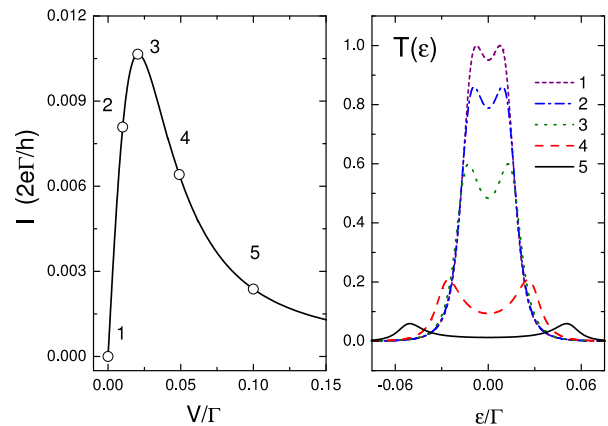


FIG. 8: (Color online) I - V characteristics for $t_c = 0.1\Gamma$ and $\Phi = 0.46\Phi_0$ (left panel). Transmission spectrum for different bias voltages for the same parameters (right panel).

eters of Fig. 8. In equilibrium ($V = 0$) a molecular state is formed. For the cases 2 and 3 the coherence is still preserved but for higher voltages (cases 4-5) the physical picture changes. In these cases, the coherence between dots is lost, the electron is localized at the left quantum dots and the molecular bridge is broken.

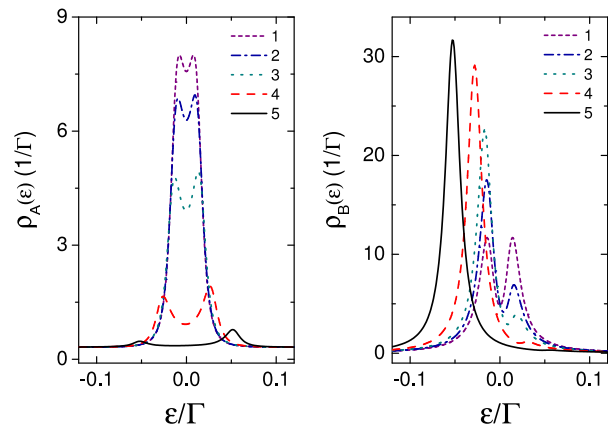


FIG. 9: (Color online) Densities of states of the electrons coming from the left at the quantum dots A (left panel) and B (right panel), for $t_c = 0.1\Gamma$ and $\Phi = 0.46\Phi_0$.

Fig. 10 shows the current versus bias voltage and magnetic flux for $t_c = 0.1\Gamma$. It can be identified clearly the two regions of maximal current at different scales. In the upper panel, there is a broad peak centered in $\Phi = 0$ and $V \approx 1.2\Gamma$. The behavior of the current versus voltage in this region was already discussed for zero flux in Fig. 7. The current maximum in this case decreases monotonously with the magnetic flux, remaining its position almost unchanged. In the same panel it is highlighted a region close to $\Phi_0/2$ and small voltages, which is plotted in the lower panel. The observed peak corresponds to the enhancement of current with the magnetic flux taking place for weak intramolecular couplings, described in Fig. 7, lower panel. The maximum of current

now occurs around $\Phi = 0.44\Phi_0$ and $V = 0.029\Gamma$. Also, this peak is clearly defined when $t_c \leq \Gamma/\sqrt{2}$, when the flux produces a total level attraction in equilibrium and it is not present when $t_c \sim \Gamma$ or larger. It is important

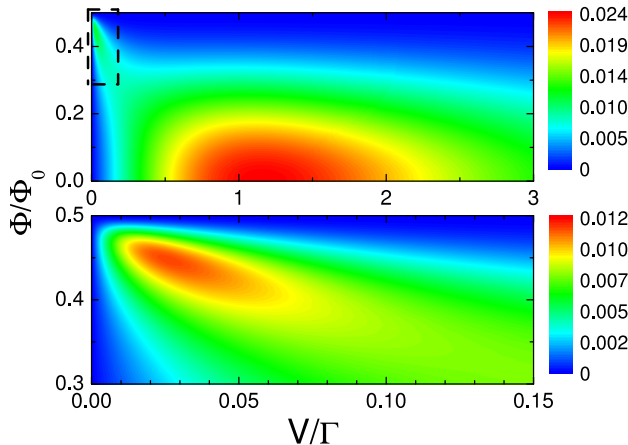


FIG. 10: (Color online) Current versus bias voltage and magnetic flux for $t_c = 0.1\Gamma$.

to note that the latter feature does not exist if the magnetic flux is absent, so that in this case we can properly talk of magnetic flux-induced NDC. Similar results are discussed in a parallel DQD molecule embedded in an Aharonov-Bohm ring¹⁹ and in a molecule in a three terminals configuration³⁶, in both cases NDC occurred in the strong interdot repulsion limit.

We expect that the above picture remains valid even if the electron-electron interaction is taken into account. In fact, in embedded QD arrays, the main effect of the electron-electron interaction is to shift and to split the resonance positions^{7, 2}. This occurs because the on-site Coulomb repulsion energy U introduces a renormalization of the site energies. In analogy with QD arrays in series, we expect that depending on the relation between the interdot coupling and the on-site Coulomb interaction different regimes arise. For $t_c/U \ll 1$, the resonances and antiresonances would split into two distinct minibands separated by the on-site Coulomb energy, while for $t_c/U \gg 1$, the resonances and antiresonances would occur in pairs. We think that the above behavior would

not break the negative differential conductance. A work in this direction is under progress.

IV. SUMMARY

We studied the transmission and the I - V characteristics for two double quantum dot molecules embedded in an Aharonov-Bohm ring. We showed that for $t_c \leq \Gamma$, the magnetic flux can be used to control totally the conductance, allowing this to take any value between 0 and $2e^2/h$. When $t_c \leq \Gamma/\sqrt{2}$ the flux produces an effective level attraction and lines of perfect transmission, allowing the levels to meet at the center of the band at a determinate value of the flux. On the other hand, the system displays BICs when $\Phi = n\Phi_0$ (n integer), and total suppression of transmission when $\Phi = n\Phi_0/2$ n odd. In the non-equilibrium regime, we identify two kind of NDC regions in the I - V characteristics, occurring at different scales and of different origin. A first current peak exists at voltages of the order of the characteristic linewidth Γ , and it is independent of the magnetic flux. The role of the flux in this case is to control the height of the overall current. The drop of current with the increase of bias has analogous explanation to the NDC region in a serial DQD. A second peak in the I - V characteristics takes place only when $t_c < \Gamma$, at voltages $V \sim \Gamma/10$ and it is strongly dependent on the magnetic flux. In fact, it does not exist if the flux is absent. The current suffers an abrupt rise for small bias voltages, as consequence of an effective level attraction of the hybridized levels produced by the flux. The decrease of current is result of the destruction of this effect when the bias is increased.

Acknowledgments

The authors acknowledge financial support from FONDECYT, under grant 1080660. M. L. L. de G. thanks financial support from Milenio ICM P06-067-F, and P. A. O. and G. A. L. from CONICYT/Programa Bicentenario de Ciencia y Tecnología (CENAVA, grant ACT27).

¹ J. R. Petta, A. C. Johnson, J. M. Taylor, E. A. Laird, A. Yacoby, M. D. Lukin, C. M. Marcus, M. P. Hanson, and A. C. Gossard, *Science* **309**, 2180 (2005); A. K. Hüttel, S. Ludwig, H. Lorenz, K. Eberl, and J. P. Kotthaus, *Phys. Rev. B* **72**, 081310(R) (2005).

² L. I. Glazman, F. W. J. Hekking, and A. I. Larkin, *Phys. Rev. Lett.* **83**, 1830 (1999); W.G. van der Wiel, S. De Franceschi, T. Fujisawa, J.M. Elzerman, S. Tarucha, and L.P. Kouwenhoven, *Science* **289**, 2105 (2000); T. H. Stievater, Xiaoqin Li, D. G. Steel, D. Gammon, D. S. Katzer, D. Park, C. Piermarocchi, and L. J. Sham, *Phys.*

Rev. Lett. **87** 133603 (2001); T. Fujisawa, D. G. Austing, Y. Tokura, Y. Hirayama, and S. Tarucha, *Nature* **419**, 278 (2002).

³ K. Ono, D. G. Austing, Y. Tokura, S. Tarucha, *Science* **297**, 1313 (2002).

⁴ A. Vidan, R. M. Westervelt, M. Stopa, M. Hanson, and C. Gossard, *Appl. Phys. Lett.* **85**, 3602 (2004).

⁵ P. Borri, S. Schneider, W. Langbein, U. Woggon, A. E. Zhukov, V. M. Ustinov, N. N. Ledentsov, Z. I. Alferov, D. Ouyang, and D. Bimberg, *Appl. Phys. Lett.* **79** 2633 (2001); A. V. Uskov, E. P. O'Reilly, M. Laemmlin, N.

- N. Ledentsov, and D. Bimberg, *Opt. Commun.* **248**, 211 (2005).
- ⁶ N. N. Ledentsov, V. M. Ustinov, A. Y. Egorov, A. E. Zhukov, M. V. Maksimov, I. G. Tabatadze, and P. S. Kopev, *Semiconductors* **28**, 832 (1994).
- ⁷ W. G. van der Wiel, S. De Franceschi, J. M. Elzerman, T. Fujisawa, S. Tarucha, and L. P. Kouwenhoven, *Rev. Mod. Phys.* **75** 1 (2003).
- ⁸ N. C. van der Vaart, S. F. Godijn, Y. V. Nazarov, C. J. P. M. Harmans, J. E. Mooij, L. W. Molenkamp, C. T. Foxon, *Phys. Rev. Lett.* **74**, 4702 (1995); F. R. Waugh, M. J. Berry, C. H. Crouch, C. Livermore, D. J. Mar, R. M. Westervelt, K. L. Campman, and A. C. Gossard, *Phys. Rev. B* **53**, 1413 (1996).
- ⁹ A. W. Holleitner, C. R. Decker, H. Qin, K. Eberl, and R. H. Blick, *Phys. Rev. Lett.* **87**, 256802 (2001).
- ¹⁰ M. L. Ladrón de Guevara, F. Claro, and P. A. Orellana, *Phys. Rev. B* **67** 195335 (2003).
- ¹¹ K. Kang and S. Y. Cho, *J. Phys. Condens. Matter* **16**, 117 (2004).
- ¹² T.-S. Kim and S. Hershfield, *Phys. Rev. B* **63**, 245326 (2001).
- ¹³ D. Boese, W. Hofstetter, and H. Schoeller, *Phys. Rev. B* **66**, 125315 (2002).
- ¹⁴ M. Sigrist, T. Ihn, K. Ensslin, D. Loss, M. Reinwald, and W. Wegscheider, *Phys. Rev. Lett.* **96**, 036804 (2006).
- ¹⁵ T. Ihn, M. Sigrist, K. Ensslin, W. Wegscheider, and M. Reinwald, *New Journal of Phys.* **9**, 111 (2007).
- ¹⁶ P. A. Orellana, M. L. Ladrón de Guevara, and F. Claro, *Phys. Rev. B* **70** 233315 (2004).
- ¹⁷ V. Moldoveanu, M. Tolea, A. Aldea, and B. Tanatar, *Phys. Rev. B* **71**, 125338 (2005).
- ¹⁸ D. Sztenkiel and R. Swirkowicz, *J. Phys.: Condens. Matter* **19**, 176202 (2007).
- ¹⁹ B. Dong, X. L. Lei, and N. J. M. Horing, *Phys. Rev. B* **77**, 085309 (2008).
- ²⁰ A. Ramsak, J. Mravlje, R. Zitko, and J. Bonca, *Phys. Rev. B* **74**, 241305(R) (2006).
- ²¹ D. Sztenkiel and R. Swirkowicz, *J. Phys.: Condens. Matter* **19**, 386224 (2007).
- ²² B. Kubala and J. König, *Phys. Rev. B* **65**, 245301 (2002).
- ²³ V. M. Apel, M. A. Davidovich, G. Chiappe, E. V. Anda, *Phys. Rev. B* **72**, 125302 (2005).
- ²⁴ J. Weis, R. J. Haug, K. v. Klitzing, and K. Ploog, *Phys. Rev. Lett.* **71**, 4019 (1993).
- ²⁵ T. C. L. G. Sollner, P. E. Tannenwald, D. D. Peck and W. D. Goodhue, *Appl. Phys. Lett.* **45**, 1319 (1984).
- ²⁶ D. Weinmann, W. Häusler, and B. Kramer, *Phys. Rev. Lett.* **74**, 984 (1995).
- ²⁷ M. Ciorga, M. Pioro-Ladriere, P. Zawadzki, P. Hawrylak, and A. S. Sachrajda, *Appl. Phys. Lett.* **80**, 2177 (2002).
- ²⁸ A. Thielmann, M. H. Hettler, J. König, and G. Schön, *Phys. Rev. B* **71**, 045341 (2005).
- ²⁹ M. C. Rogge, F. Cavaliere, M. Sassetti, R. J. Haug, and B. Kramer, *New J. Phys.* **8** 298 (2006).
- ³⁰ R. Aguado and D. C. Langreth, *Phys. Rev. Lett.* **85**, 1946 (2000).
- ³¹ G. A. Lara, P. A. Orellana, and E. V. Anda, *Solid State Commun.* **125**, 165 (2003).
- ³² J. Fransson and O. Eriksson, *J. Phys.: Condens. Matter* **16**, L85 (2004); J. Fransson and O. Eriksson, *Phys. Rev. B* **70**, 085301 (2004).
- ³³ B. Wunsch, M. Braun, J. König, and D. Pfannkuche, *Phys. Rev. B* **72**, 205319 (2005).
- ³⁴ V. H. Nguyen, V. L. Nguyen, and P. Dollfus, *Appl. Phys. Lett.* **87**, 123107 (2005).
- ³⁵ J. N. Pedersen, B. Lassen, A. Wacker, and M. H. Hettler, *Phys. Rev. B* **75**, 235314 (2007).
- ³⁶ L. G. Mourkh and A. Y. Smirnov, *Phys. Rev. B* **72**, 033310 (2005).
- ³⁷ G. A. Lara, P. A. Orellana, and E. V. Anda, *Phys. Rev. B* **78**, 045323 (2008).
- ³⁸ Y.-X. Li, H.-Y. Choi, and H.-W. Lee, *Phys. Lett. A* **372**, 2073 (2008).